ADVANCES IN ATMOSPHERIC SCIENCES, VOL. 31, MARCH 2014, 305–315

Idealized Numerical Simulations of Tropical Cyclone Formation Associated with Monsoon Gyres

LIANG Jia[1,2], WU Liguang*[1,2], and ZONG Huijun[1,2]

[1]*Key Laboratory of Meteorological Disasters of the Ministry of Education, Nanjing University of Information Science and Technology, Nanjing* 210044

[2]*State Key Laboratory of Severe Weather, Chinese Academy of Meteorological Sciences, Beijing* 100081

(Received 23 November 2012; revised 7 May 2013; accepted 22 May 2013)

ABSTRACT

Monsoon gyres have been identified as one of the important large-scale circulation patterns associated with tropical cyclone (TC) formation in the western North Pacific. A recent observational analysis indicated that most TCs form near the center of monsoon gyres or at the northeast end of the enhanced low-level southwesterly flows on the southeast–east periphery of monsoon gyres. In the present reported study, idealized numerical experiments were conducted to examine the tropical cyclogenesis associated with Rossby wave energy dispersion with an initial idealized monsoon gyre.

The numerical simulations showed that the development of the low-level enhanced southwesterly flows on the southeast–east periphery of monsoon gyres can be induced by Rossby wave energy dispersion. Mesoscale convective systems emerged from the northeast end of the enhanced southwesterly flows with mid-level maximum relative vorticity. The simulated TC formed in the northeast of the monsoon gyre and moved westward towards the center of the monsoon gyre. The numerical experiment with a relatively smaller sized initial monsoon gyre showed the TC forming near the center of the initial monsoon gyre. The results of the present study suggest that Rossby wave energy dispersion can play an important role in TC formation in the presence of monsoon gyres.

Key words: monsoon gyre, tropical cyclone formation, idealized numerical simulation

Citation: Liang, J., L. G. Wu, and H. J. Zong, 2014: Idealized numerical simulations of tropical cyclone formation associated with monsoon gyres. *Adv. Atmos. Sci.*, **31**(2), 305–315, doi: 10.1007/s00376-013-2282-1.

1. Introduction

Tropical cyclone (TC) formation involves a series of complex processes by which a warm-core, TC-scale cyclonic vortex with maximum sustained wind of more than 17.2 m s^{-1} near the surface forms in the tropics. Apart from a necessary pre-existing low-level cyclonic disturbance, climatological conditions for TC formation, as identified by Gray (1968), include warm SSTs above 26.5°C, with a deep mixed layer; a conditionally unstable atmosphere; weak vertical shear; a moist mid-troposphere; and the presence of moist convection. While these requirements are generally met much of the time (Simpson et al., 1997), studies have shown that TC formation in the western North Pacific is closely associated with large-scale flow patterns (e.g., Ramage, 1974; Briegel and Frank, 1997; Ritchie and Holland, 1999; Frank and Roundy, 2006). Understanding the roles of these large-scale flow patterns in TC formation is currently a topic of active research.

Ritchie and Holland (1999) examined relationships between tropical cyclogenesis and associated large-scale patterns in the western North Pacific and identified five characteristic patterns for TC formation: (1) a monsoon shear line; (2) a monsoon confluence region; (3) a monsoon gyre; (4) easterly waves; and (5) Rossby wave energy dispersion associated with pre-existing TCs. In the 8-yr analysis, they found that 82% of TC formations were associated with a general pattern consisting of monsoonal southwesterlies and trade easterlies. Their results generally agreed with previous studies regarding the confluence zone being a favorable region for TC formation (Sadler, 1975; Frank, 1982; Briegel and Frank, 1997). Frank and Roundy (2006) examined the relationship between TC formation and tropical wave activity, including Rossby-gravity waves, tropical depression-type or easterly waves, equatorial Rossby waves, Kelvin waves, and the Madden–Julian oscillation, and suggested that all of these wave types except Kelvin waves play an important role in TC formation in the six global basins by providing a favorable environment. Bessafi and Wheeler (2006) and Molinari et al. (2007) analyzed the role of equatorial Rossby waves in TC formation over the Indian Ocean and the western North Pacific, respectively. They argued that the convection and cyclonic vorticity associated with equatorial Rossby waves are important for modulating TC formation.

* Corresponding author: WU Liguang
Email: liguang@nuist.edu.cn

In addition to providing favorable environmental conditions for TC formation, two mechanisms regarding how large-scale monsoonal flows lead to TC formation in the western North Pacific have been put forward. The first is associated with the breaking of tropical waves. Recently, Gall et al. (2010) and Gall and Frank (2010) conducted idealized numerical experiments to examine the role of equatorial Rossby waves in tropical cyclogenesis, indicating that the breaking of equatorial Rossby waves can organize the cyclonic vorticity on the TC scale and then lead to tropical cyclogenesis in the presence of an idealized monsoon trough. These studies argued that the wave-breaking mechanism is largely a downscale process. The other is associated with scale interactions, which emphasizes the interaction between mesoscale convective systems and the large-scale environment (Holland, 1995; Simpson et al., 1997; Ritchie and Holland, 1999; He et al., 2012a, 2012b). Since TC formation usually occurs in the confluence region between the monsoonal southwesterlies and the trade easterlies, Holland (1995) suggested that the confluence region can trap tropical waves in the lower troposphere through an accumulation of wave energy, as described by Chang and Webster (1990). This process can maintain and enhance tropical convection, leading to long-lived convection that frequently organizes into mesoscale convective systems in the confluence region. The latter can develop mid-level, mesoscale vortices that have been considered as key components of TC formation (e.g., Ritchie and Holland, 1997; Simpson et al., 1997). Compared to the first mechanism, an upscale energy transfer process is involved in the scale interaction theory.

In a recent observational study, Wu et al. (2013) examined monsoon gyre activity, the composited structure, and the associated TC formation during the period 2000–10. The 31 monsoon gyres identified were accompanied by the formation of 43 TCs, accounting for 20.3% of total TCs during May–October. The maximum winds of the composited monsoon gyre occurred 500–800 km away from the center with a magnitude of 8–13 m s^{-1} at 850 hPa. Extending about 1000 km outward from the center at lower levels, the cyclonic circulation of the composited monsoon gyre shrank with height and was replaced with negative vorticity above 200 hPa. Under the influence of the upper-level anticyclone and relatively weak vertical wind shears, most of the TCs associated with monsoon gyres formed near the centers of monsoon gyres and the northeast end of the enhanced southwesterly flows. While the tropical cyclogenesis associated with the energy dispersion of pre-existing TCs has been investigated (Li and Fu, 2006; Ge et al., 2008), little is known about how the energy dispersion of monsoon gyres plays a role in TC formation. Motivated by this, we report in the present paper the results of idealized numerical experiments that were performed to demonstrate the role of Rossby wave energy dispersion in TC formation in the presence of monsoon gyres.

2. Experimental design

The idealized numerical experiments were conducted using version 2.2.1 of the Advanced Research Weather Research and Forecasting (WRF-ARW) model. A single model domain with a uniform grid spacing of 30 km was centered at 20°N, including 301 × 301 grid points (9000 × 9000 km^2) and 31 vertical levels from the surface to 50 hPa. To reduce artificial wave reflection into the model interior, open lateral boundary conditions were used in the simulation. The model physics included the Kain–Fritch cumulus scheme (Kain and Fritch, 1993), the Yonsei University PBL scheme (Noh et al., 2003), the Monin–Obukhov surface layer scheme (Monin and Obukhov, 1954), the Dudhia shortwave parameterization scheme (Dudhia, 1989), and the Rapid Radiative Transfer Model (RRTM) longwave parameterization scheme (Mlawer et al., 1997).

The model was initialized with a symmetric monsoon gyre centered at 20°N (Fig. 1a). Its initial maximum tangen-

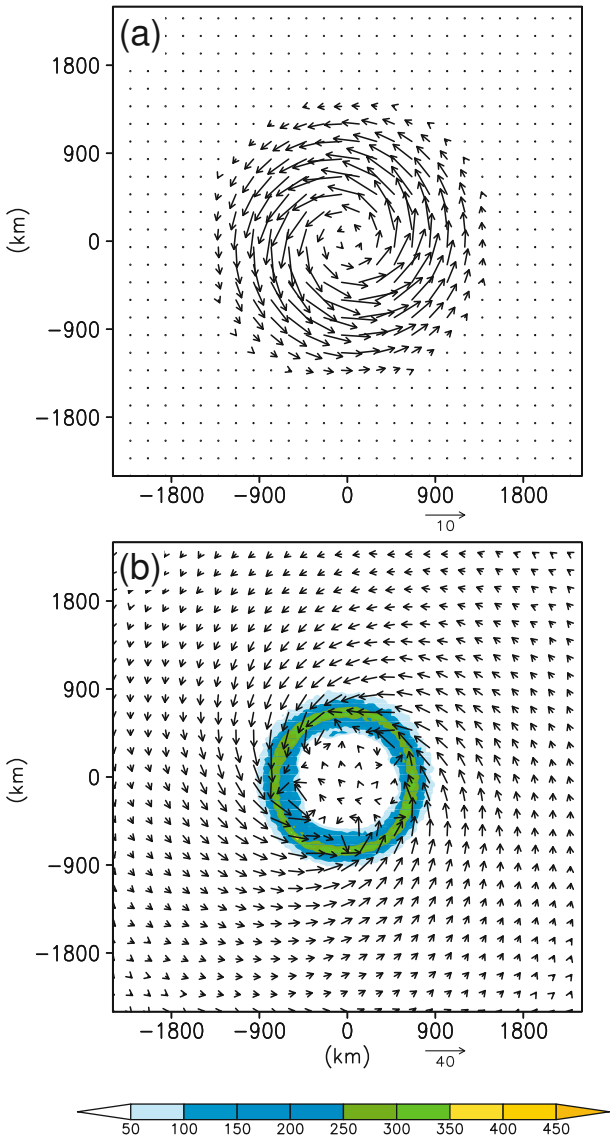

Fig. 1. (a) 700-hPa wind field (m s^{-1}, vector) of the initial monsoon gyre in all experiments, and (b) 700-hPa wind field (m s^{-1}, vector) of the monsoon gyre and accumulated rainfall (mm, shading) simulated in the numerical experiment on the f-plane at 120 h.

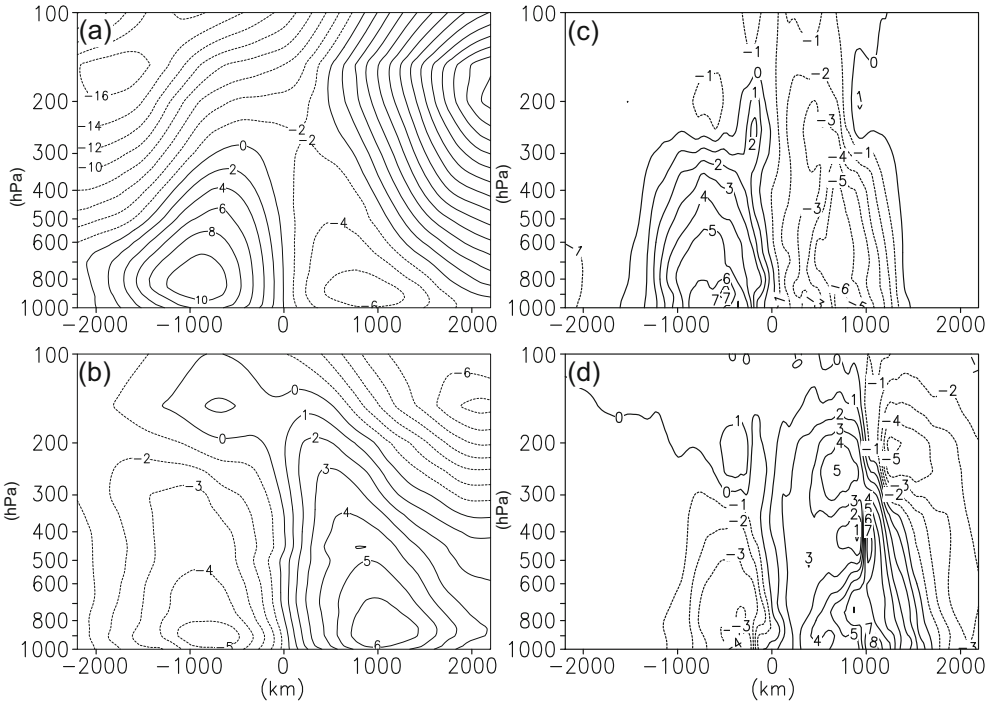

Fig. 2. The (a, b) composited and (c, d) simulated vertical profiles of (a, c) zonal and (b, d) meridional winds (m s^{-1}) with contour intervals of 2.0 in (a) and 1.0 m s^{-1} in (b–d).

tial wind was 10 m s^{-1} at a radius of 600 km from the gyre center, and gradually decreased in the vertical direction to zero at 100 hPa. As a result, the idealized monsoon gyre was initially characterized by cyclonic circulation below 100 hPa and a weak warm core at around 600 hPa. The initial monsoon gyre was embedded in a quiescent atmospheric environment over an open ocean with a constant SST of 29°C.

The control experiment (CTRL) was run on the β-plane, in which the size of the initial monsoon gyre was 3000 km in diameter. To examine the capability of the model and the associated model physics, the experiment was also run on the f-plane. In doing so, no Rossby wave energy dispersion should have occurred, and the monsoon gyre should not have moved due to a lack of the planetary vorticity gradient or the beta effect (Carr and Elsberry, 1995). As shown in Fig. 1b, the monsoon gyre was able to fairly maintain its symmetric structures in terms of wind and rainfall without significant movement. In addition, sensitivity experiments were also performed. In one sensitivity experiment, the size of the initial monsoon gyre was set to be 2000 km in order to examine the possible influence of the monsoon gyre size (S2000), while in the other sensitivity experiment a nested domain with 10-km spacing was used to examine the influence of the model resolution on the simulated TC structure. Here, we focus mainly on the Rossby wave energy dispersion and associated tropical cyclogensis in the CTRL experiment.

3. Numerical results from the CTRL experiment

3.1. *Simulated TC activity*

During the first 48-h integration, the initially axisymmetric monsoon gyre gradually evolved with vertical structure features similar to those observed (Fig. 2), which were composited from 36 monsoon gyres that occurred during the period 2000–10. With a size of about 4000 km, the composited monsoon gyre showed cyclonic circulation below 250 hPa and anticyclonic circulation above 250 hPa. Maximum winds were found at a radius of 700–900 km at lower levels (Figs. 2a and b).

Figure 3 shows the early 72-h evolution of 700-hPa streamlines and wind speeds associated with the initially symmetric monsoon gyre shown in Fig. 1a, suggesting that the low-level features of the induced Rossby wave energy dispersion were similar to the barotropic case in Carr and Elsberry (1995). By 24 h, the initial symmetry of the monsoon gyre became distorted due mainly to the β-effect (Fig. 3a). The elongated (compressed) streamlines can be taken mainly as a manifestation of the β-induced troughing (ridging) to the west (east). The southerly winds were enhanced in the eastern semicircle between the monsoon gyre and the induced anticyclonic circulation (A). As the distortion occurred, the streamlines and isolines of vorticity were no longer parallel, and the resulting advection of relative vorticity led to two anticyclones (Fig. 3b). While the northern anticyclone (A1) was associated with the so-called β-gyres that can lead to the propagation of the monsoon gyre (Wang, 1998), the occurrence of the southeastern anticyclone (A) was attributed to Rossby wave energy dispersion (Chan and Williams, 1987; Shapiro and Ooyama, 1990; Luo, 1994). By 72 h (Fig. 3c), A1 had shifted farther to the northwest, and the development of the wave train could be seen in the southeast quadrant (Chan and Williams, 1987; Luo, 1994). Li et al. (2003) suggested that the larger (smaller) meridional (zonal) length

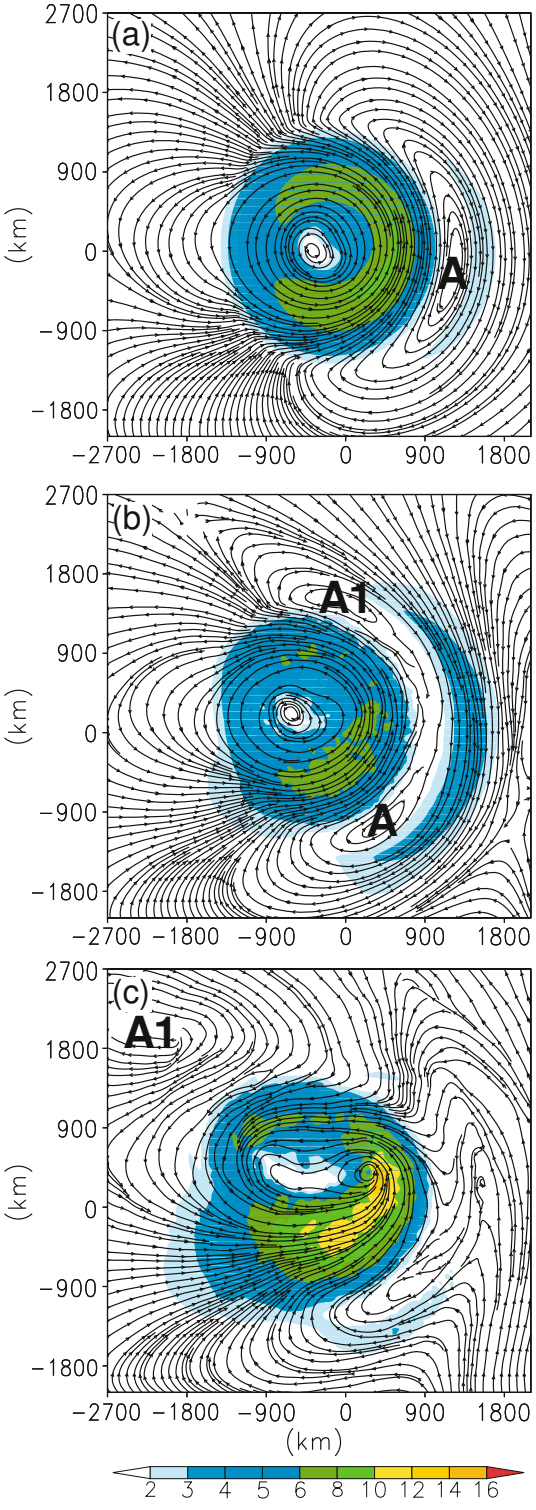

Fig. 3. Simulated 700-hPa streamline patterns and wind speeds (m s^{-1}, shading) at (a) 24 h, (b) 52 h, and (c) 72 h in the CTRL experiment with A and A1 indicating anticyclonic circulations.

scale of the wave train is essential for southeastward energy propagation. They argued that wave energy propagates eastward with respective to the mean flow when the meridional wavelength exceeds the zonal wavelength. It can be seen that the southwesterly winds were further enhanced between the monsoon gyre and the resulting anticyclonic circulation.

Compared to the lower-level flow pattern, the upper-level circulation became rather complicated. Figure 4a shows the simulated 200-hPa wind field and wind speeds that exceeded 20 m s^{-1} at 72 h. With a maximum of about 32 m s^{-1}, the strongest outflows associated with the upper-level anticyclone that surrounded a cyclonic circulation lay to the east of the low-level enhanced southwesterly winds. The simulated flow patterns were generally similar to the composited wind fields in Wu et al. (2013), except for the 850-hPa trade winds and 200-hPa mid-latitude westerly flows, which were not included in the idealized experiments in the present study.

The formation of the simulated TC was associated with the enhanced southwesterly winds and rainfall on the eastern side of the monsoon gyre (Fig. 4b). The TC reached tropical storm intensity at 82 h when it was located at about 500 km

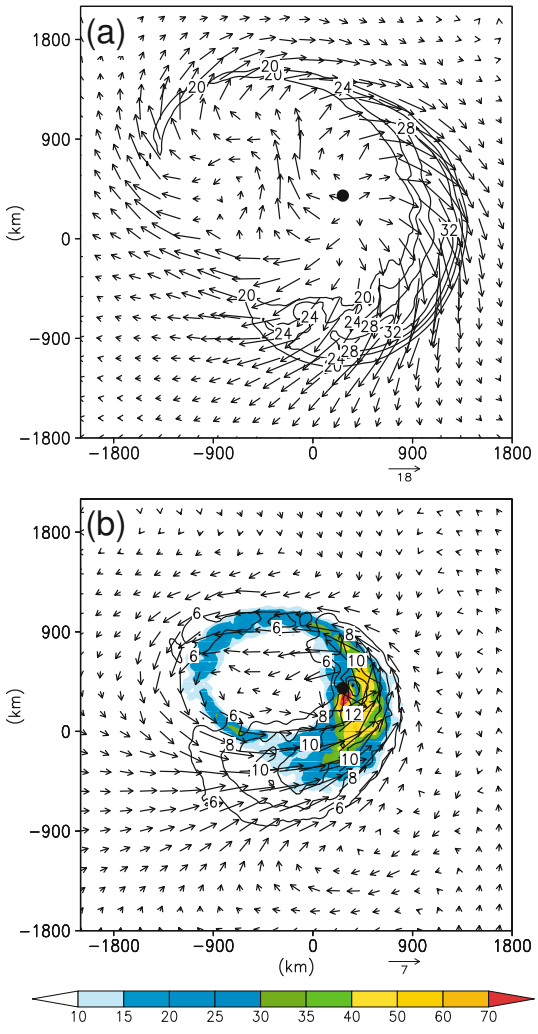

Fig. 4. Simulated (a) 200-hPa wind field (m s^{-1}, vector) and wind speed (m s^{-1}, contour) with intervals of 4 m s^{-1}, and (b) 700-hPa wind field (m s^{-1}, vector) and wind speed (m s^{-1}, contour) with intervals of 2.0 m s^{-1}, and accumulated rainfall (mm, shading) at 72 h in the CTRL experiment. Accumulated rainfall less than 10 mm is suppressed and closed dots denote the center of the disturbance.

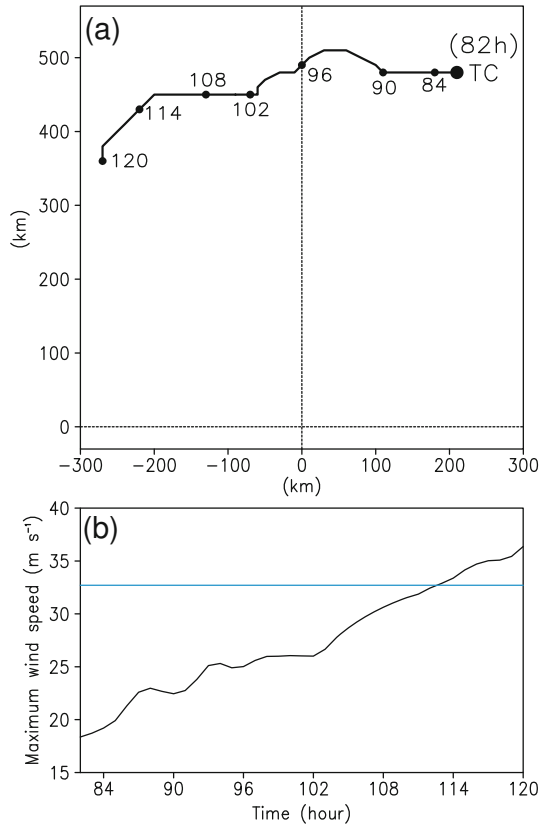

Fig. 5. Simulated (a) track and (b) intensity (m s^{-1}) evolution of the TC in the CTRL experiment. The blue solid line in (b) indicates the maximum wind speed of 32.7 m s^{-1}.

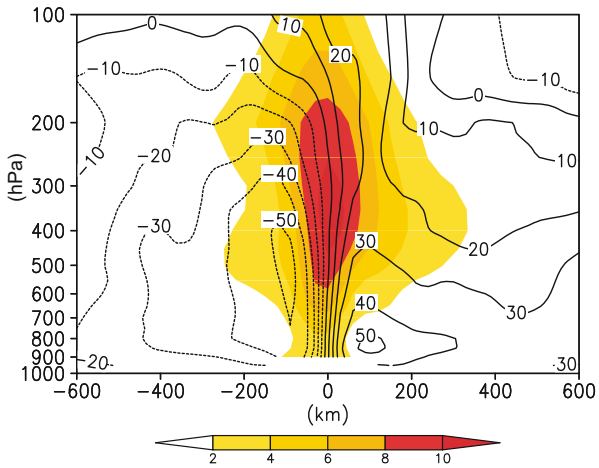

Fig. 6. Vertical cross section of the meridional wind component (m s^{-1}, contour) and temperature anomaly (K, shading) across the center of the simulated TC at 120 h in the CTRL experiment. The contour interval is 10 m s^{-1}.

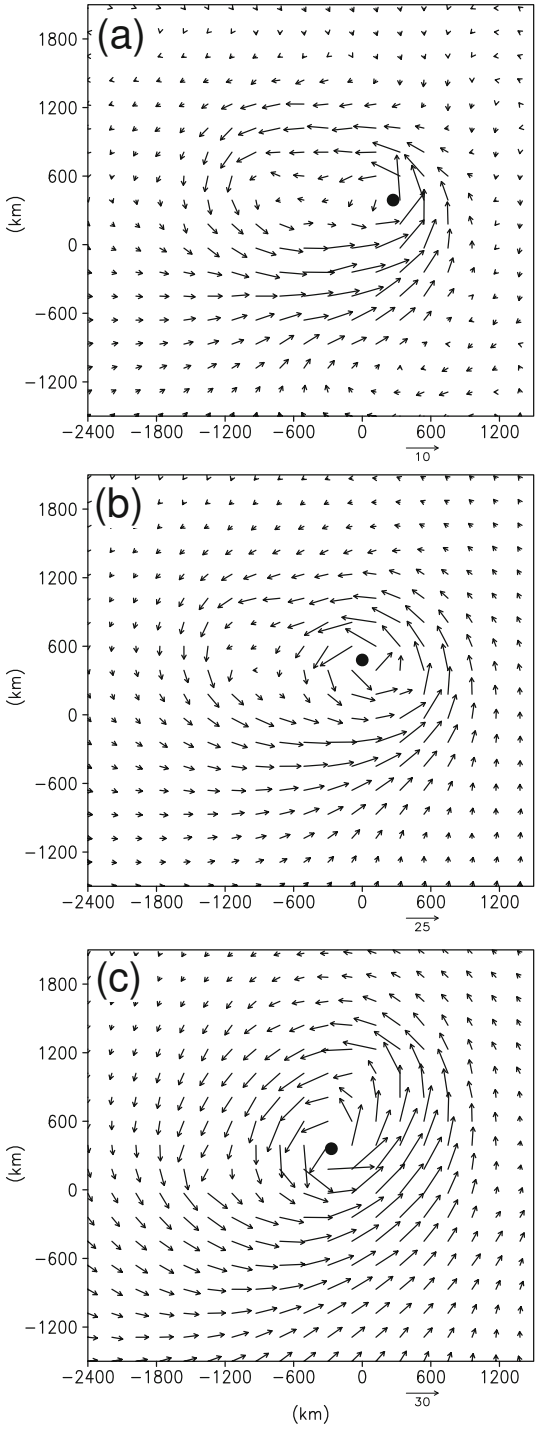

Fig. 7. Simulated 700-hPa wind fields (m s^{-1}) at (a) 72 h, (b) 96 h, and (c) 120 h in the CTRL experiment. The black dots indicate the center of the TC.

northeast of the center of the initial monsoon gyre (Fig. 5a). The development of the TC was associated with the northeast end of the enhanced southwesterly flows in an environment with relatively small vertical wind shear (Fig. 4). The TC continued to intensify and reached typhoon strength at 113 h, moving westward along the northern periphery of the monsoon gyre by 120 h (Figs. 5a and 5b). Figure 6 shows the vertical structure of the simulated TC at 120 h, suggesting that the simulated TC had a typical structure of a mature TC. The maximum winds in the TC occurred 100 km away from the TC center near 800 hPa, with a warm core of 10 K at about 350 hPa.

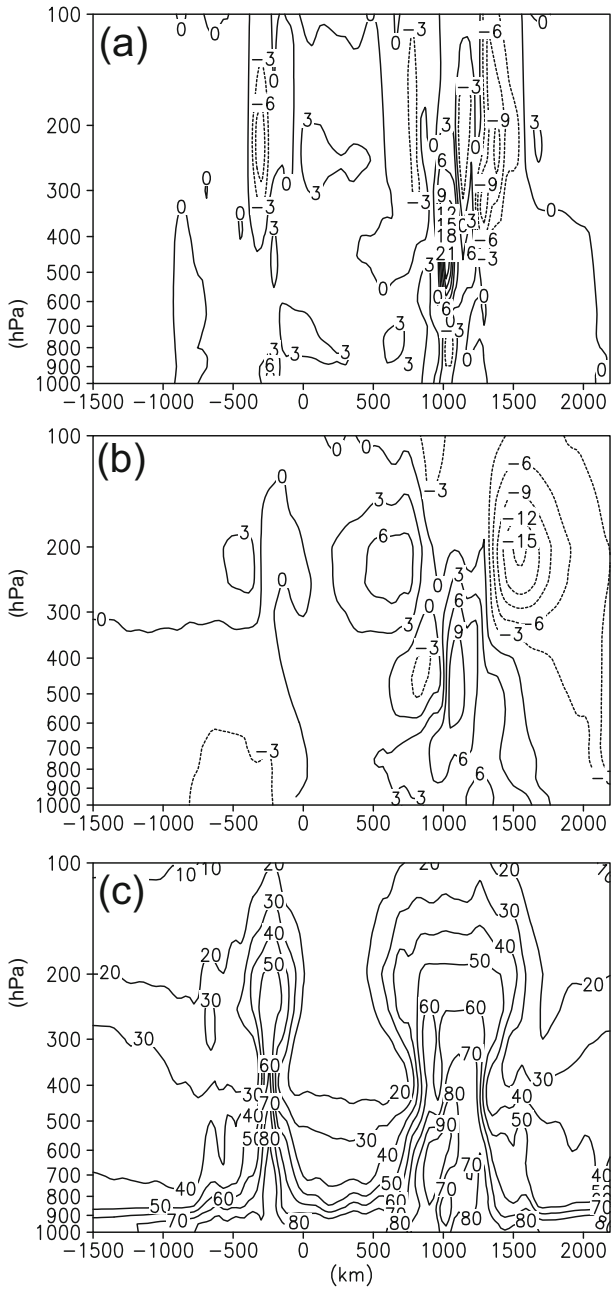

Fig. 8. Vertical cross sections of (a) relative vorticity (10^{-5} s^{-1}), (b) meridional wind component (m s^{-1}), and (c) relative humidity (%) across the center of the monsoon gyre at 60 h in the CTRL experiment.

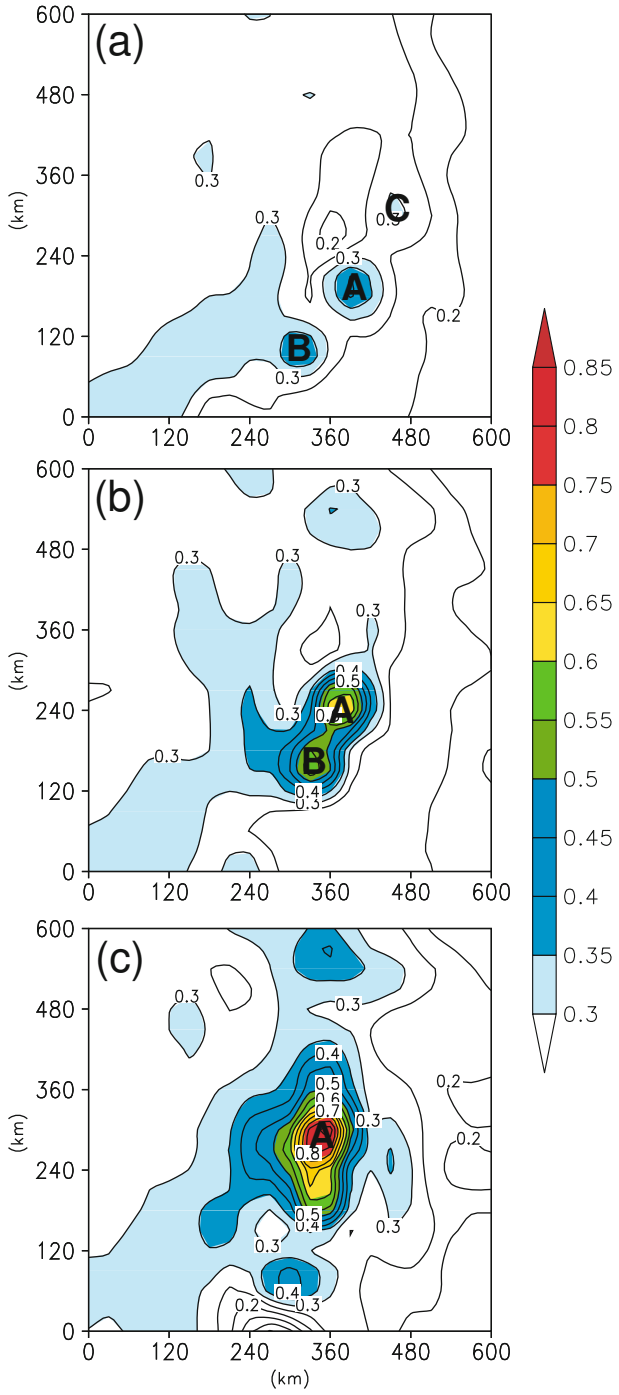

Fig. 9. Simulated 600-hPa potential vorticity (PVU) at (a) 52 h, (b) 55 h, and (c) 58 h in the CTRL experiment. The shaded areas indicate the potential vorticity exceeding 0.3 PVU with A, B, and C indicating the potential vorticity maxima.

Of note is that the westward motion of the simulated TC was accompanied by significant changes in the wind field. At 72 h, the presence of the simulated TC led to an elongated monsoon gyre in the west–east direction, while the strong southwesterly winds extended farther northeastward on the southeast–east periphery of the monsoon gyre (Fig. 7a). As the simulated TC moved westward, its center was collocated with the center of the monsoon gyre at around 120 h, leading to an elongated monsoon gyre in the southeast–northeast direction (Figs. 7b and c).

3.2. *Simulated tropical cyclogenesis*

Mapes and Houze (1995) examined the vertical profiles of mean horizontal divergence in tropical oceanic mesoscale convective systems and found that most of the profiles can be classified as convective divergence profiles and stratiform divergence profiles in the troposphere. The convective (stratiform) divergence profiles consist of the conver-

gence in the lower (mid) troposphere and divergence in the upper (upper and lower) troposphere, typically associated with deep convective (stratiform) precipitation. Several previous studies have suggested that tropical cyclogenesis is closely associated with the transformation from stratiform divergence profiles to convective divergence profiles (Bister and Emanuel, 1997; Ritchie and Holland, 1997; Simpson et al., 1997). Ritchie and Holland (1997) examined the synoptic and mesoscale conditions during the pre-formation and formation periods of Typhoon Irving (1992) using synoptic and research aircraft data and suggested that a cooperative scale interaction played an important role in the formation of the typhoon.

Figure 8 shows the vertical cross section of relative vorticity, meridional wind component and relative humidity along a west–east line across the monsoon gyre center at 60 h, 22 hours before the simulated TC reached tropical storm intensity. As in the composited analysis in Wu et al. (2013), the monsoon gyre was dominated by positive and negative relative vorticity at lower and upper levels, respectively. Large values of positive vorticity could be found about 1000 km away from the initial center of the monsoon gyre at around 500 hPa (Fig. 8a). In the meridional wind component (Fig. 8b), the mid-level cyclonic vorticity corresponded with southerly and northerly winds on the east and west sides of the vorticity maximum, suggesting the development of a tropical disturbance at middle levels. The tropical disturbance could be clearly seen in the 500-hPa wind field (not shown). The relative humidity was about 80% at middle levels (Fig. 6c), providing favorable conditions for the development of the tropical disturbance.

Simpson et al. (1997) and Ritchie and Holland (1997) argued that interactions between mesoscale convective systems may play an important role in tropical cyclogenesis. The merger of several mesoscale convective systems can make a vortex develop vertically by increasing the horizontal size of the potential vorticity (PV) perturbation and its magnitude, both of which lead to an increase in the penetration depth of the PV perturbation (Hoskins et al., 1985). In terms of 600-hPa potential vorticity, Fig. 9 displays the merger of mesoscale vorticity perturbations from 52 h to 60 h. At 52 h (Fig. 9a), we can identify three potential vorticity perturbations in the region of the enhanced southwesterly winds. At this time, the horizontal size of the PV was about 100 km. At 55 h and 58 h (Figs. 9b and c), it can be seen that the merger of these perturbations increased the horizontal size and magnitude of the PV.

To illustrate the influence of the merger process, the relative vorticity and divergence profiles were averaged over an area of 120×120 km^2, centered at the 600-hPa maximum vorticity (Fig. 10). At 60 h, the positive vorticity extended from 800 hPa to 200 hPa with a maximum at 500 hPa, and weak negative vorticity could be found below 800 hPa. The lower-level negative vorticity disappeared and maximum vorticity was lowered to 600 hPa at 72 h. In association with the downward displacement of the maximum relative vorticity, the divergence profiles showed transformation from a stratiform divergence profile to a convective divergence profile. As shown in Fig. 10b, at 60 h the convergence between 800 hPa and 400 hPa was coupled with upper- and lower-tropospheric divergence, indicating a stratiform divergence profile. Twelve hours later, lower tropospheric convergence and upper tropospheric divergence indicated a convective divergence profile.

We also calculated each term in the vorticity equation and

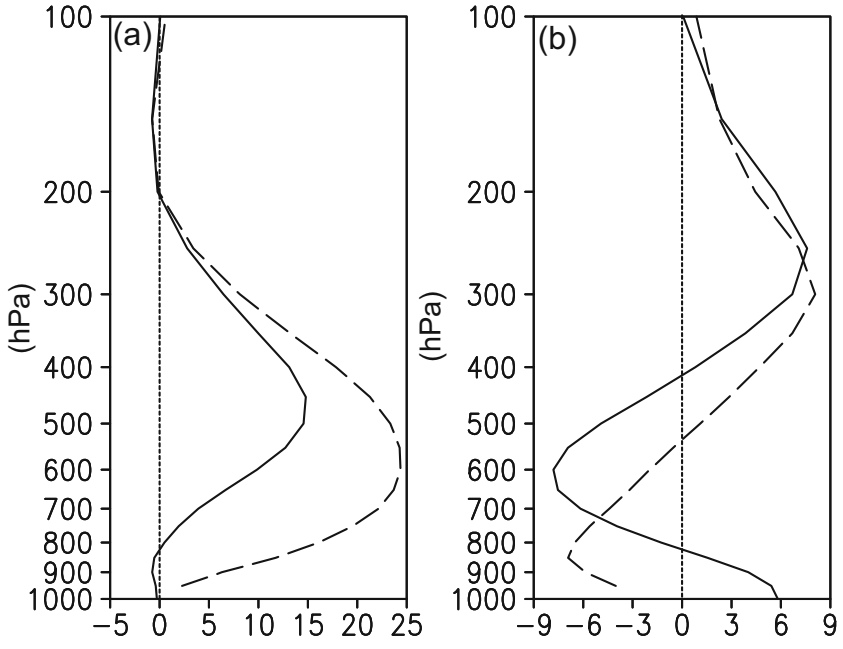

Fig. 10. Vertical profiles of (a) relative vorticity (10^{-5} s^{-1}) and (b) divergence (10^{-5} s^{-1}) averaged over an area of 120×120 km centered at the 600-hPa vorticity maximum at 60 h (solid) and 72 h (dashed) in the CTRL experiment.

averaged them over a 120×120 km area centered at the 600-hPa vorticity maximum. At $t = 60$ h (Fig. 11a), the positive vorticity tendency extended from 850 hPa to 150 hPa, with a maximum at 400 hPa. The negative vorticity tendency occurred below 850 hPa. The budget calculation clearly indicated that the positive vorticity tendency was mainly from the stretching and tilting terms below (above) 450 hPa. In other words, the increasing cyclonic vorticity in the middle troposphere was associated with the increasing convergence. At 72 h (Fig. 11b), the positive vorticity tendency appeared below 400 hPa, with a maximum at 700 hPa. While the advection terms still dominated the positive vorticity tendency above 600 hPa, the enhancing cyclonic circulation in the lower troposphere arose from the stretching and tilting terms. In agreement with Simpson et al. (1997) and Ritchie and Holland (1997), the development of the simulated TC started from the middle troposphere and was associated with the merger of mesoscale convective systems.

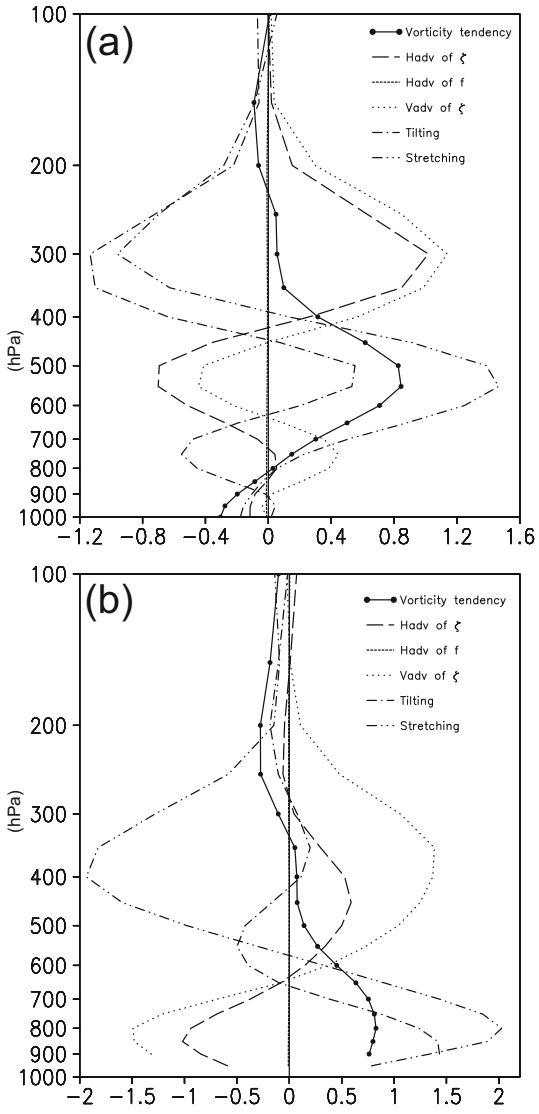

Fig. 11. Vertical profiles of the total vorticity tendency and individual contributions (10^{-8} s^{-2}) averaged over an area of 120×120 km centered at the 600-hPa vorticity maximum at (a) 60 h, and (b) 72 h in the CTRL experiment.

4. Sensitivity experiments

In Wu et al. (2013), it was shown that TC formation seems to be related to the size of the initial monsoon gyre. Figure 12 shows the 72-h evolution of the monsoon gyre in the experiment, in which the size of the initial monsoon gyre was 2000 km in diameter. The pattern of the enhanced southwesterly winds to the southeast of the monsoon gyre center was very similar to that in the CTRL experiment, apart from relatively weak anticyclonic circulation to the northeast of the monsoon gyre.

In this experiment, a TC formed in the southeast–east periphery of the enhanced southwesterly winds of the monsoon gyre, close to the center of the monsoon gyre about 150 km northeast, and reached tropical storm strength at 80 h, slightly earlier than the simulated TC in the CTRL experiment (Fig. 13). In addition, the TC moved northward and then northwestward, which was mainly steered by the flows associated with the monsoon gyre (Fig. 13a). It is therefore suggested that the size of the monsoon gyre is one of the important parameters controlling the genesis location.

As shown in Fig. 6, the radii of maximum wind at 120 h were about 100 km for the simulated TC in the CTRL experiment. Although it had a typical structure of mature TCs, the eye size of the simulated TC was a little large compared to observations (Weatherford and Gray, 1988). To examine whether the eye size depends on the horizontal resolution, we conducted a numerical experiment with a nested domain to cover the activity of the simulated TC. The spacing of the nested domain was 10 km with 301×301 grids. In addition to the model physics used in the coarse domain, the Lin et al. (1983) microphysics scheme was used in the nested domain, which included six classes of hydrometeors: water vapor, cloud water, rain, cloud ice, snow, and grauple (Lin et al., 1983; Rutledge and Hobbs, 1984; Chen and Sun, 2002). The nested domain started at 72 h and ran for 48 hours.

Figure 14 shows the simulated TC structure with the 10-km nested domain. Compared to Fig. 6, the eye size of the simulated TC was reduced significantly to about 50 km, suggesting an influences of the coarse resolution and/or the microphysics scheme on the structure of the simulated TC.

5. Summary

Monsoon gyres have been identified as one of the important large-scale circulation patterns associated with TC formation in the western North Pacific (e.g., Lander, 1994; Ritchie and Holland, 1999; Chen et al., 2004). In Wu et al. (2013), observational analysis indicated that most TCs form near the centers of monsoon gyres and the northeast end of the enhanced lower-level southwesterly flows on the southeast periphery of the monsoon gyre. Thus, numerical experiments were conducted to examine the role of Rossby wave

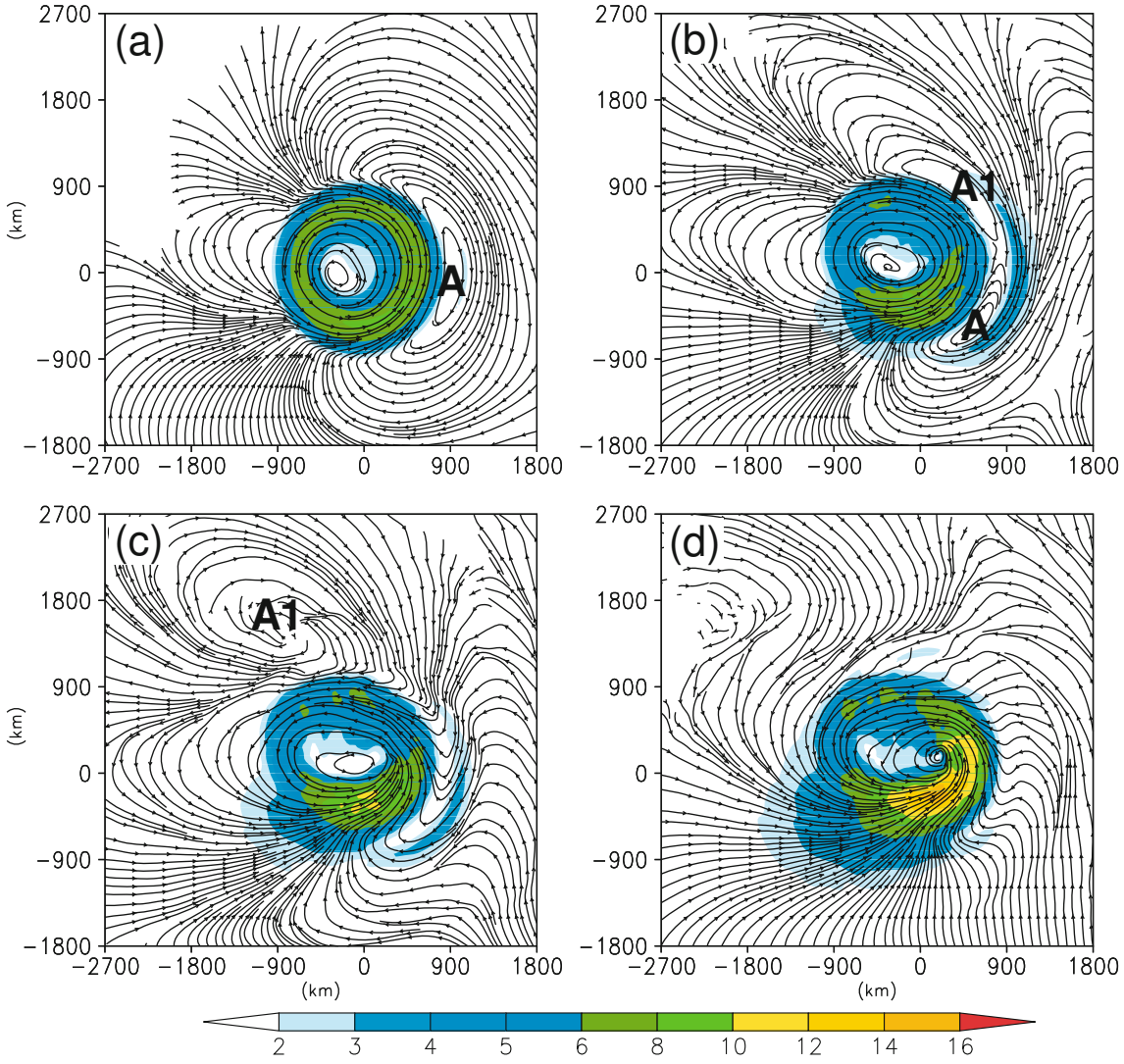

Fig. 12. Simulated 700-hPa streamline patterns and wind speeds (m s^{-1}, shading) at (a) 24 h, (b) 56 h, (c) 64 h, and (d) 72 h in the S2000 experiment with A and A1 indicating anticyclonic circulations.

energy dispersion with an initial idealized monsoon gyre.

The WRF model was initialized with a symmetric monsoon gyre that was characterized by cyclonic circulation below 100 hPa and a weak warm core around 600 hPa. The initial monsoon gyre was embedded in a quiescent atmospheric environment at a constant SST of 29°C. Three numerical experiments were conducted and the results described. The first numerical experiment was run on the f-plane and no Rossby wave energy dispersion associated with the monsoon gyre was observed. The second (CTRL) and third experiments (S2000) were run on the β-plane. The numerical simulations showed that the development of the lower-level enhanced southwesterly flows on the south-southeast periphery of monsoon gyres can be induced by Rossby wave energy dispersion.

In the CTRL experiment, mesoscale convective systems emerged from the northeast end of the enhanced southwesterly flows with mid-level maximum relative vorticity and the simulated TC formed at 82 h in the northeast of the monsoon gyre. The S2000 experiment, with a relatively smaller size of the initial monsoon gyre, showed a simulated TC forming slightly earlier in association with the enhanced southwesterly flows, and was located much closer to the center of the initial monsoon gyre. The results suggests that Rossby wave energy dispersion plays an important role in TC formation associated with monsoon gyres.

Note that the present study does not exclude the possible role of tropical waves in TC formation (e.g., Frank and Roundy, 2006; Bessafi and Wheeler, 2006; Molinari et al., 2007) through the wave-breaking mechanism, as described by Gall et al. (2010) and Gall et al. (2010), or through scale interactions (Holland, 1995; Simpson et al., 1997; Ritchie and Holland, 1999). In the absence of tropical waves, our numerical experiments suggested that TC formation can occur due to Rossby wave energy dispersion associated with monsoon gyres. In addition, due to the coarse horizontal resolution used, high-resolution numerical simulations should be conducted to study the

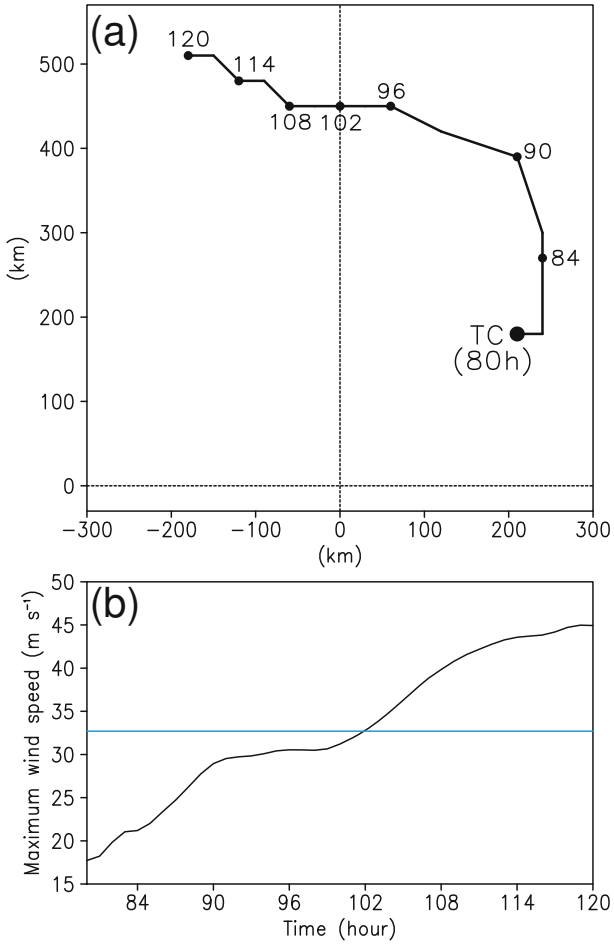

Fig. 13. Simulated (a) track and (b) intensity (m s^{-1}) evolution of the TC in the S2000 experiment. The blue solid line in (b) indicates the maximum wind speed of 32.7 m s^{-1}.

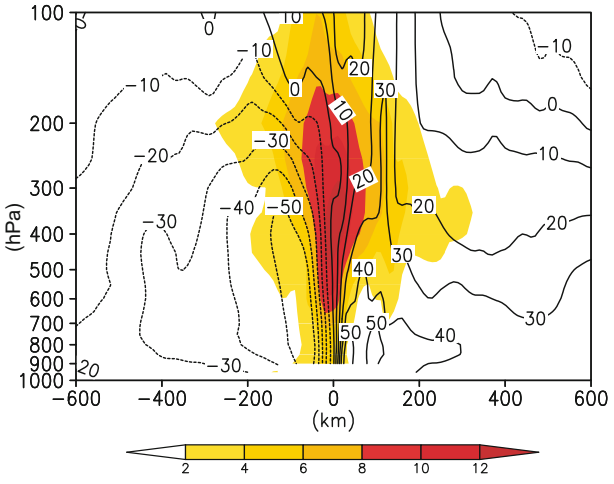

Fig. 14. Vertical cross section of the meridional wind component (m s^{-1}, contour) and temperature anomaly (K, shading) across the centers of the simulated TC at 120 h in the 10-km domain (CTRL). The contour interval is 10 m s^{-1}.

subject of tropical cyclogenesis. The detailed processes involved in TC formation collectively represent the focus of our ongoing research.

Acknowledgements. This research was jointly supported by the typhoon research project (Grant No. 2009CB421503) of the National Basic Research Program of China, the National Natural Science Foundation of China (Grant No. 41275093), the social commonwealth research program of the Ministry of Science and Technology of the People's Republic of China (Grant No. GYHY200806009), and the Priority Academic Program Development of Jiangsu Higher Education Institutions (PAPD).

REFERENCES

Bessafi, M., and M. C. Wheeler, 2006: Modulation of south Indian Ocean tropical cyclones by the Madden-Julian oscillation and convectively coupled equatorial waves. *Mon. Wea. Rev.*, **134**, 638–656.

Bister, M., and K. A. Emanuel, 1997: The genesis of hurricane guillermo: TEXMEX analyses and a modeling study. *Mon. Wea. Rev.*, **125**, 2662–2682.

Briegel, L. M., and W. M. Frank, 1997: Large-scale influences on tropical cyclogenesis in the western North Pacific. *Mon. Wea. Rev.*, **125**, 1397–1413.

Carr, L. E., and R. L. Elsberry, 1995: Monsoonal interactions leading to sudden tropical cyclone track changes. *Mon. Wea. Rev.*, **123**, 265–290.

Chan, J. C. L., and R. T. Williams, 1987: Analytical and numerical studies of the beta-effect in tropical cyclone motion. Part I: Zero mean flow. *J. Atmos. Sci.*, **44**, 1257–1265.

Chang, H. R., and P. J. Webster, 1990: Energy accumulation and emanation at low latitudes. Part II: Nonlinear response to strong episodic equatorial forcing. *J. Atmos. Sci.*, **47**, 2624–2644.

Chen, S.-H., and W.-Y. Sun, 2002: A one-dimensional time dependent cloud model. *J. Meteor. Soc. Japan*, **1**, 99–118.

Chen, T. C., S.-Y. Wang, M.-C. Yen, and W. A. Gallus Jr., 2004: Role of the monsoon gyre in the interannual variation of tropical cyclone formation over the western North Pacific. *Wea. Forecasting*, **19**, 776–785.

Dudhia, J., 1989: Numerical study of convection observed during the winter monsoon experiment using a mesoscale two-dimensional model. *J. Atmos. Sci.*, **46**, 3077–3107.

Frank, W. M., 1982: Large-scale characteristics of tropical cyclones. *Mon. Wea. Rev.*, **110**, 572–586.

Frank, W. M., and P. E. Roundy, 2006: The role of tropical waves in tropical cyclogenesis. *Mon. Wea. Rev.*, **134**, 2397–2417.

Gall, J. S., and W. M. Frank, 2010: The role of Equatorial Rossby Waves in tropical cyclogenesis. Part II: idealized simulations in a monsoon trough environment. *Mon. Wea. Rev.*, **138**, 1383–1398.

Gall, J. S., W. M. Frank, and M. C. Wheeler, 2010: The role of Equatorial Rossby Waves in Tropical cyclogenesis. Part I: Idealized numerical simulations in an initially quiescent background environment. *Mon. Wea. Rev.*, **138**, 1368–1382.

Ge, X. Y., T. Li, Y. Q. Wang, and M. S. Peng, 2008: Tropical cyclone energy dispersion in a three-dimensional primitive equation model: Upper tropospheric influence. *J. Atmos. Sci.*, **65**, 2272–2289.

Gray, W. M., 1968: Global view of the origin of tropical disturbances and storms. *Mon. Wea. Rev.*, **96**, 669–700.

He, G. X., G. Li, X. L. Zou, and P. S. Ray, 2012a: Applications of a velocity Dealiasing scheme to data from the China new generation weather radar system (CINRAD). *Wea. Forecasting*, **27**, 218–230.

He, G. X., G. Li, X. L. Zou, and P. S. Ray, 2012b: A velocity Dealiasing scheme for synthetic C-band data from China's new generation weather radar system (CINRAD). *J. Atmos. Oceanic Technol.*, **29**, 1263–1274.

Holland, G. J., 1995: Scale interaction in the Western Pacific monsoon. *Meteor. Atmos. Phys.*, **56**, 57–79.

Hoskins, B. J., M. E. McIntyre, and A. W. Robertson, 1985: On the use and significance of isentropic potential vorticity maps. *Quart. J. Roy. Meteor. Soc.*, **111**, 877–846.

Kain, J. S., and J. M. Fritch, 1993: Convective parameterization for mesoscale models: The Kain-Fritch scheme. *The Representation of Cumulus Convection in Numerical Models, Meteor. Monogr.*, No. 46, Amer. Meteor. Soc., 165–170.

Lander, M. A., 1994: Description of a monsoon gyre and its effects on the tropical cyclones in the western North Pacific during August 1991. *Wea. Forecasting*, **9**, 640–654.

Li, T., and B. Fu, 2006: Tropical cyclogenesis associated with Rossby wave energy dispersion of a preexisting typhoon. Part I: Satellite data analyses. *J. Atmos. Sci.*, **63**, 1377–1389.

Li, T., B. Fu, X. Ge, B. Wang, and M. Peng, 2003: Satellite data analysis and numerical simulation of tropical cyclone formation. *Geophys. Res. Lett.*, **30**, 2122, doi: 10.102a/2003GL018556.

Lin, Y.-L., R. D. Farley, and H. D. Orville, 1983: Bulk parameterization of the snow field in a cloud model. *J. Climate Appl. Meteor.*, **22**, 40–63.

Luo, Z. X., 1994: Effect of energy dispersion on the structure and motion of tropical cyclone. *Acta Meteor. Sinica*, **8**, 51–59.

Mapes, B. E., and R. A. Houze, 1995: Diabatic divergence profiles in Western Pacific mesoscale convective systems. *J. Atmos. Sci.*, **52**, 1807–1828.

Mlawer, E. J., S. J. Taubman, P. D. Brown, M. J. Iacono, and S. A. Clough, 1997: Radiative transfer for inhomogeneous atmospheres: RRTM, a validated correlated-k model for the longwave. *J. Geophys. Res.*, **102**(D14), 16 663–16 682.

Molinari, J., K. Lombardo, and D. Vollaro, 2007: Tropical cyclogenesis within an Equatorial Rossby wave packet. *J. Atmos. Sci.*, **64**, 1301–1317.

Monin, A. S., and A. M. Obukhov, 1954: Basic laws of turbulent mixing in the atmosphere near the ground. *Tr. Akad. Nauk SSSR Geofiz. Inst.*, **64**, 1963–1987.

Noh, Y., W. G. Cheon, S.-Y. Hong, and S. Raasch, 2003: Improvement of the K-profile model for the planetary boundary layer based on large eddy simulation data. *Bound.-Layer Meteor.*, **107**, 401–427.

Ramage, C. S., 1974: The typhoons of October 1970 in the South China Sea: Intensification, decay and ocean interaction. *J. Appl. Meteor.*, **13**, 739–751.

Ritchie, E. A., and G. J. Holland, 1997: Scale interactions during the formation of Typhoon Irving. *Mon. Wea. Rev.*, **125**, 1377–1396.

Ritchie, E. A., and G. J. Holland, 1999: Large-scale patterns associated with tropical cyclogenesis in the Western Pacific. *Mon. Wea. Rev.*, **127**, 2027–2043.

Rutledge, S. A., and P. V. Hobbs, 1984: The mesoscale and microscale structure and organization of clouds and precipitation in midlatitude cyclones. XII: a diagnostic modeling study of precipitation development in narrow cold-frontal rainbands. *J. Atmos. Sci.*, **41**, 2949–2972.

Sadler, J. C., 1975: The monsoon circulation and cloudiness over the GATE Area. *Mon. Wea. Rev.*, **103**, 369–387.

Shapiro, L. J., and K. V. Ooyama, 1990: Barotropic vortex evolution on a beta plane. *J. Atmos. Sci.*, **47**, 170–187.

Simpson, J., E. Ritchie, G. J. Holland, J. Halverson, and S. Stewart, 1997: Mesoscale interactions in tropical cyclone genesis. *Mon. Wea. Rev.*, **125**, 2643–2661.

Wang, Y. P., 1998: On the bogusing of tropical cyclones in numerical models: The influence of vertical structure. *Meteor. Atmos. Phys.*, **65**, 153–170.

Weatherford, C. L., and W. M. Gray, 1988: Typhoon structure as revealed by aircraft reconnaissance. Part II: Structural variability. *Mon. Wea. Rev.*, **116**, 1044–1056.

Wu, L. G., H. J. Zong, and J. Liang, 2013: Observational analysis of tropical cyclone formation associated with monsoon gyres. *J. Atmos. Sci.*, **70**, 1023–1034.